Journal of King Saud University – Engineering Sciences 32 (2020) 368–377

Contents lists available at ScienceDirect

Journal of King Saud University – Engineering Sciences

journal homepage: www.sciencedirect.com

Original article

Modeling of an intelligent battery controller for standalone solar-wind hybrid distributed generation system

Partha Sarothi Sikder, Nitai Pal *

Department of Electrical Engineering, Indian Institute of Technology (Indian School of Mines), Dhanbad, Jharkhand 826004, India

ARTICLE INFO

Article history:
Received 21 May 2018
Accepted 14 February 2019
Available online 19 February 2019

Keywords:
Renewable energy
Solar
Wind
MPPT
Hybrid
Power quality

ABSTRACT

In this paper, a different approach of standalone hybrid distributed generation has been shown. Due to the intermittent nature of the renewable energy resources, the reliability of the power system is decreased using single renewable energy source based electricity supply system. To overcome the problem the size of the storage system exceptionally large which increases the overall cost of the system and drastically reduces the flexibility. To resolve the problem a standalone hybrid power supply system is designed by integrating the solar and wind energy to generate electricity. The hybrid system increases the generation capacity without increasing the storage unit and maintains reliable electricity to the consumer. The proposed system has been modelled using Matlab/Simulink and verify under variable sources and load condition without compromising with the power quality issue.

1. Introduction

At present, due to population outbreak the day to day energy demand has been increased which affect the resources of conventional energy sources, as the major amount of generated electricity has come from the fossil fuel (Zoua et al., 2016). Generally after generating the electricity fossil fuel is exhausted. By increasing the capacity of generation of electricity using fossil fuel enhances the depletion fuel resources. So to compensate the future energy demand the only alternative is the renewable energy sources, which does not exhausted after generation of electricity (Panwar et al., 2011). On the other hand, during generation of electricity the fossil fuel emits harmful gases to the environment and pollutes our environment. Hence, to protect our environment and support the nation's sustainable development the renewable energy sources got the prime attention to generate electricity. A standalone distributed generation system is effective for electrifying a remote rural area where traditional grid connection is absent (Jamal et al., 2017). Due to the absence of the grid connectivity the battery maintains the reliability of the supplied electricity. The battery stores the generated electricity during the availability of the renewable energy sources and the stored energy supplied to the consumer whenever required. The integration of different renewable energy sources reduces the dependency on the battery and increased the overall generating capacity without increasing the size of the energy storage unit. The present study is addressing a new technology to integrate the generated electricity from solar and wind energy sources in a standalone distributed generation system to ensure optimum reliability to the consumer.

2. Proposed configuration

The proposed configuration of a standalone hybrid power supply system (SHPSS) is shown in Fig. 1.

In this proposed system, both the solar energy and the wind energy is converted to electrical energy using PV array and a wind turbine generator (WTG) set. An incremental conductance (IC) based maximum power point tracking (MPPT) controller is attached to the PV array to maintain the power at the maximum power level during variable solar irradiance and then, the obtained energy is supplied to the battery bank. For WTG the optimum torque controlled (OTC) based MPPT controller is maintaining the maximum power level under variable wind speed. To store the generated AC from the WTG a three phase rectifier unit is attached to the system which converts generated AC to DC and then, the obtained energy is supplied to the battery bank. In this proposed system to store the generated energy from solar and wind, individ-

* Corresponding author.
E-mail address: nitai@iitism.ac.in (N. Pal).
Peer review under responsibility of King Saud University.

Production and hosting by Elsevier

https://doi.org/10.1016/j.jksues.2019.02.002
1018-3639/

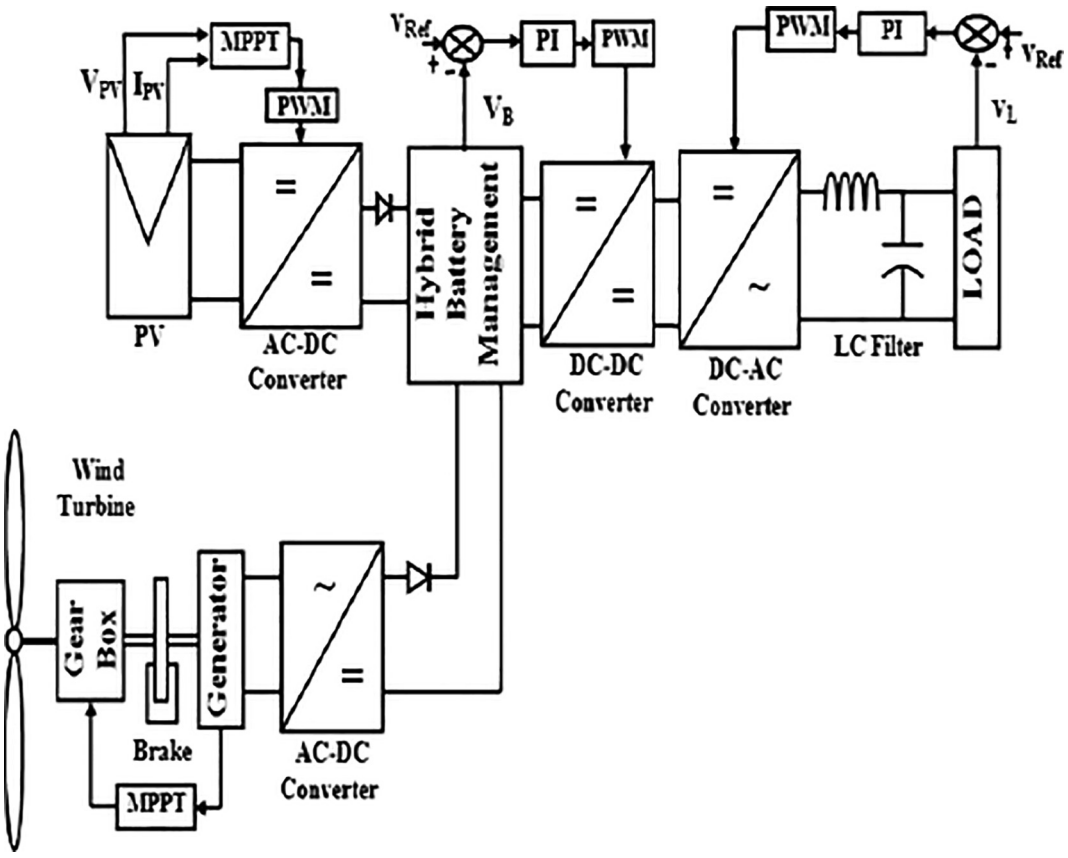

Fig. 1. A standalone hybrid power supply system using solar and wind energy.

ual battery bank is connected to the individual sources separately and the generated energy is supplied to the load using a hybrid battery management system. The charge controller maintains the battery management system in such a way that a single battery unit is in operation at a time and the other remains in standby condition. The voltage of the operating battery is increased using stepped up DC-DC converter and further converted to AC with the desired quality using a PI controlled DC-AC inverter to maintain desired voltage.

2.1. Photovoltaic cell circuit diagram and performance

The solar irradiance is directly converted to electricity using photovoltaic (PV) cell. A PV model using the data of Sun Power E20/435 W has been built in MATLAB Simulation software (https://us.sunpower.com). The I-V and P-V characteristic of the array are shown in Figs. 2 and 3 considering the temperature of the environment is constant.

2.2. Buck converter

To maintain the generated voltage at the maximum power level a buck converter is utilised here operated by the incremental conductance (IC) based MPPT controller. In a buck converter the semiconductor switch continuously turns ON and OFF by the switching signals provided by the MPPT controller to maintain the desired output voltage at the maximum level. The inductor and capacitor are applied here to maintain the current and voltage ripple within the limit. The output voltage of the buck converter is

$$V_{out} = DV_{in} \quad (1)$$

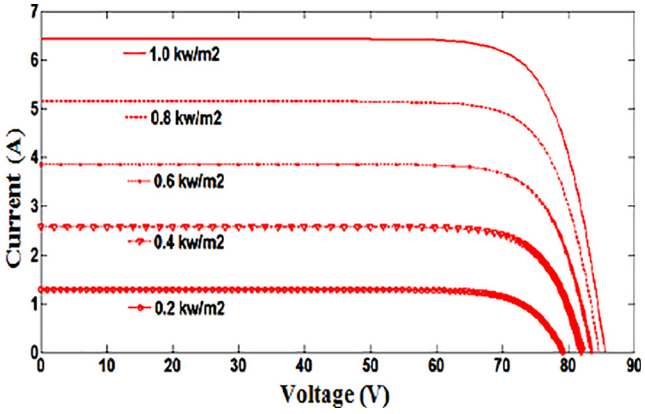

Fig. 2. I-V curve of PV array.

where, V_{in} is the input voltage of the Buck converter, V_{out} is the output voltage of the buck converter and D represents the duty cycle (Rashid, 2007).

2.3. Incremental conductance (IC) method

In this proposed system to extract power under variable irradiance of the sun the incremental conductance (IC) based MPPT controller is used here. To obtain maximum power the voltage and the current is observed and the conductance of the network is analysed. The maximum power is obtain by changing the duty cycle of the controller and by maintain desired voltage (Ebrahimi, 2015; Kamran et al., 2018). The driving equation of the IC based MPPT method is

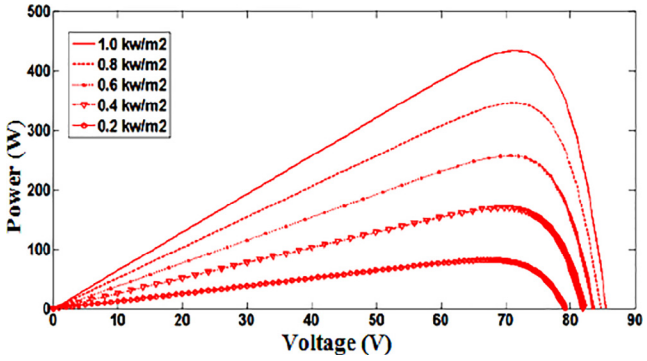

Fig. 3. P-V curve of PV array.

$$\frac{dP}{dV} = \frac{d(VI)}{dV} = I + V\frac{dI}{dV} = 0 \tag{2}$$

Fig. 4 indicates the voltage vs power profile of a PV array under a constant solar irradiance. Due to variation of voltage the extracting power also changes. The PV array provides the maximum power when $\frac{dp}{dv} = 0$.

From the figure if the operating voltage of the PV array is less than the maximum power condition voltage the Eq. (2) modifies to

$$\frac{dI}{dV}\rangle - \frac{I}{V};\left(\frac{dP}{dV}\rangle 0\right) \tag{3}$$

which indicates the less power drown by the PV array with less voltage. But whenever the operating voltage is too high the PV array again draws less amount of power and the Eq. (2) modifies to

$$\frac{dI}{dV}\langle - \frac{I}{V};\left(\frac{dP}{dV}\langle 0\right) \tag{4}$$

The Eq. (3) indicates left hand side of the maximum power condition and Eq. (4) satisfies the right hand side of the MPP condition observed in Fig. 4.

The algorithm related to IC based MPPT controller is shown in Fig. 5. Where k represents the counter and D represents the duty cycle which operates the connected DC to DC converter to maintain the maximum power condition. During operation the duty cycle, is simultaneously changed to obtain the MPP condition at different irradiance as well as temperature under variable load condition also.

Here, the counter senses the present voltage V (k) and I (k) and compute the conductance. Based on the measured conductance the duty cycle changes to reach the MPP based on the network conductance indicated in Eqs. (2)–(4).

2.4. Power generation from wind using wind turbine

Wind Turbine (WT) converts the wind energy to the mechanical torque, which rotates the shaft of an electrical generator to generate electrical energy (Taleb, 2004; Zammit et al., 2017; Hur, 2018). The power generated by the wind turbine is

$$P_w = 0.5AC_p(\lambda,\beta)\times(V_\omega)^3 \tag{5}$$

where,

P, air density (kilograms per cubic meter); V_ω, wind speed in meters per second; A, blades' swept area; C_p, turbine-rotor-power coefficient; λ, tip-speed ratio; β, pitch angle. The maximum power is found using maximum power point tracking algorithm (MPPT) is used to capture maximum energy from the fluctuating wind speed. And the tip-speed ratio is defined as

$$\lambda = \frac{\omega_\omega R}{V_\omega} \tag{6}$$

where, ω_ω is the angular velocity of rotor [rad/s], R is the rotor radius [m] and V_ω is the wind speed upstream of the rotor [m/s].

The C_p–λ characteristics, for different values of the pitch angle β, are illustrated in Fig. 6 From the characteristic of C_p–λ it is evident that the maximum value of turbine-rotor-power coefficient (C_p) is achieved for β = 0°. The profile of the power of the wind turbine is dependents on the turbine speed which is shown in Fig. 7.

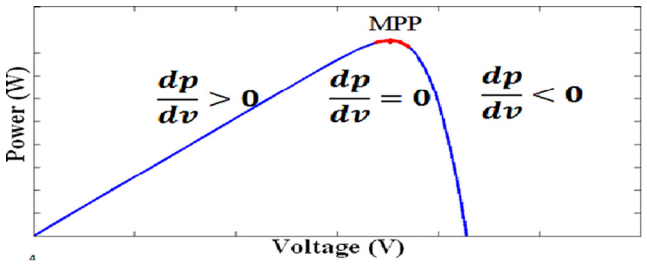

Fig. 4. Operating power (P) and voltage (V) curve of the conventional IC algorithm.

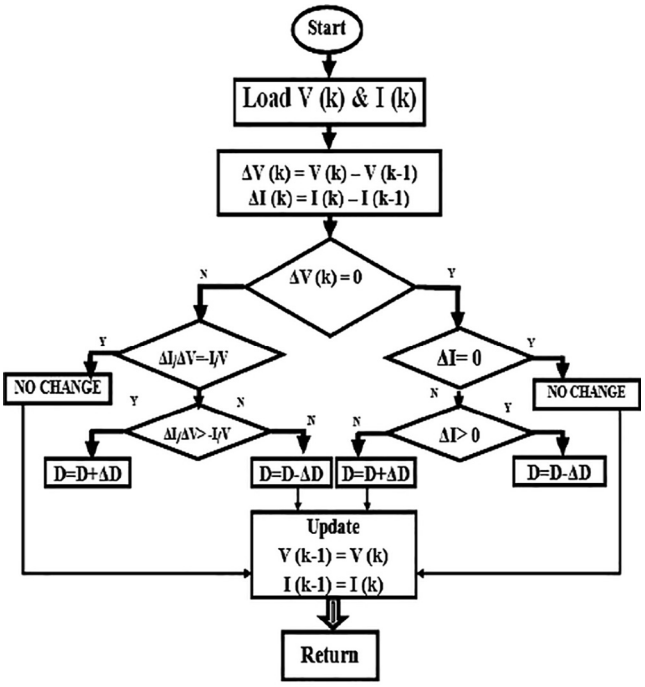

Fig. 5. Incremental Conductance (IC) algorithm for MPPT controller.

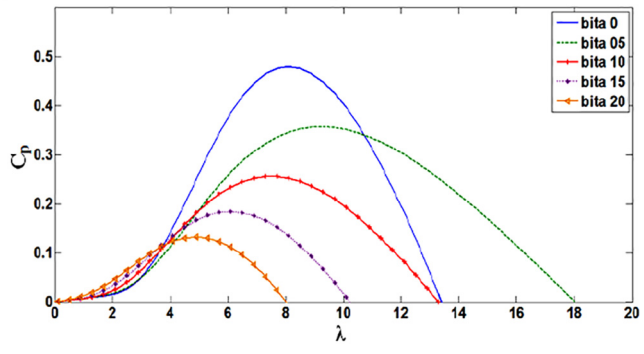

Fig. 6. Analytical approximation of Cp (λ, β) characteristics.

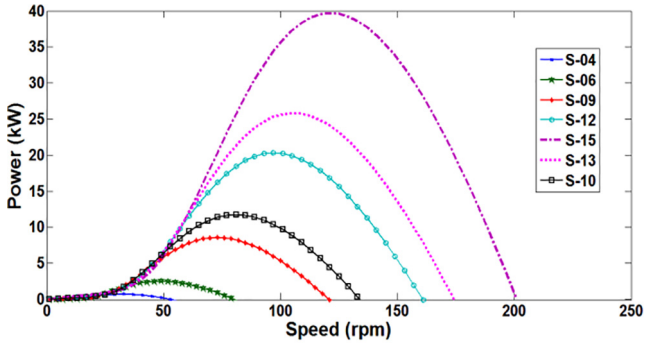

Fig. 7. Electrical power generated by the turbine as a function of the rotor speed for different wind speeds.

2.5. Mathematical model of PMSM

PMSG is considered as the most promising technologies for variable speed wind energy conversion systems. In order to design the PMSG the mathematical model of the motor the space vector form of the stator voltage equation have been derived in Eq. (7) (Zhihui et al., 2009; Arifujjaman, 2010; Wu et al., 2013)

$$v_s^{abc} = R_s i_s^{abc} + \frac{d}{dt}\psi_s^{abc} \tag{7}$$

where R_s is the stator winding resistance per phase, I_s^{abc} is the stator phase current, V_s^{abc} is the stator phase voltage and Ψ_s^{abc} is the flux linkage.

A transformation from abc to synchronous dq reference frame is needed in order to have a simpler model that will be simulated in Matlab/Simulink. The model is derived in dq reference frame were q axis is rotating with 90° ahead to the d axis with respect to the direction of rotation is defined as

$$v_{sd} = R_s i_{sd} + \frac{d}{dt}\psi_{sd} - p\omega_m\psi_{sq} \tag{8}$$

$$v_{sq} = R_s i_{sq} + \frac{d}{dt}\psi_{sq} + p\omega_m\psi_{sd} \tag{9}$$

where v_{sd}, v_{sq} are the dq axis stator voltage, i_{sd}, i_{sq} are the dq axis stator current, Ψ_{sd}, Ψ_{sq} are the dq axis stator flux linkages, R_s stator resistances and ω_m is the mechanical speed in rad/s. P is the no of pole.

Flux linkage equations are expressed as presented in Eqs. (10) and (11).

$$\psi_{sd} = L_d I_{sd} + \psi_m \tag{10}$$

$$\psi_q = L_q I_{sq} \tag{11}$$

with $L_d = L_q = L_s$ dq axis inductances and Ψ_m permanent magnet flux linkage. With the help of flux linkage equations, stator voltage equations in dq reference frame have the fallowing form:

$$v_{sd} = R_s i_{sd} + L_d\frac{d}{dt}i_{sd} - p\omega_m L_q i_{sq} = R_s i_{sd} + L_s\frac{d}{dt}i_{sd} - p\omega_m L_s i_{sq} \tag{12}$$

$$\begin{aligned} v_{sq} &= R_s i_{sq} + L_q\frac{d}{dt}i_{sq} + p\omega_m(L_d i_{sd} + \psi_m) \\ &= R_s i_{sq} + L_s\frac{d}{dt}i_{sq} + p\omega_m(L_d i_{sd} + \psi_m) \end{aligned} \tag{13}$$

The torque equation of PMSG can be derived from the power balance equation. The power owing into the machine can be express in dq reference frame as presented in Eq. (14)

$$P_{se} = \frac{3}{2}\left[v_{sd}i_{sd} + v_{sq}i_{sq}\right] \tag{14}$$

After substituting the stator voltage equations and the flux equation in dq reference frame in Eq. (14) and separating the power quantities the power has the fallowing form:

$$P_{se} = \frac{3}{2}\left[\left(R_s i_{sd}^2 + R_s i_{sq}^2\right) + L_s\left(\frac{d}{dt}i_{sd}^2 + \frac{d}{dt}i_{sq}^2\right) + p\omega_m\left(\Psi_{sd}i_{sq} - \Psi_{sq}i_{sd}\right)\right] \tag{15}$$

The first term represents the power loss in the conductors, the second term indicates the time rate of change of storing energy in the magnetic fields and the third term express the energy conversion, from electrical energy to mechanical energy. From the third term can be express the electromagnetic torque because the power output from the motor shaft must be equal to the electromechanical power.

$$P_e = \omega_m T_e = \frac{3}{2}\left[\omega_e\Psi_{sd}i_{sq} - \omega_e\Psi_{sq}i_{sd}\right] \tag{16}$$

The relation between the electrical velocity and the mechanical angular velocity of the motor depends on the number of pole pairs as presented below

$$\omega_e = p\omega_m \tag{17}$$

If in the Eq. (21) the expression of flux is replaced by the Eqs. (9) and (10) then the torque will have the following form

$$T_e = \frac{3}{2}p\left[\Psi_m i_{sq} + (L_d - L_q)i_{sd}i_{sq}\right] \tag{18}$$

In the final expression of the torque, Eq. (18), it can be observed that there are two terms, the first one represents the synchronous torque and is produced by the flux of the permanent magnets and the second term represents the reluctance torque and represents the torque produced by the difference of the inductances in dq reference frame. In the project the motor is surface mounted permanent magnet and in this case the inductances in dq reference frame are equal resulting a simpler expression of the electromagnetic torque, without the reluctance torque. With the assumption expressed above, the Eq. (18) has the following form

$$T_e = \frac{3}{2}p\left[\Psi_m i_{sq}\right] \tag{19}$$

The mechanical equation of the machine is expressed as a function of the electromagnetic torque (T_e), load torque (T_l) and electrical velocity of the machine:

$$T_e = T_l + B\omega_m + J\frac{d\omega_m}{dt} \tag{20}$$

where J is the moment of inertia and B is the viscous friction.

2.6. Optimal torque control (OTC)

In case of OTC MPPT methodology the generator torque is adjusted to its optimal value at different wind speeds. However, it requires the knowledge of the turbine characteristics ($C_{p\max}$ and λ_{opt}) (Xiaodong et al., 2013; Jena and Rajendran, 2015).

If the conditions are optimal, based on Eq. (6), the optimum speed of the rotor can be estimated as

$$\omega_{m_o pt} = \frac{v_\omega.\lambda_{opt}}{R} = K_w v_\omega. \tag{21}$$

Combining Eqs. (5) and (21) yields the optimum mechanical power generated by the wind turbine is

$$P_{w_o pt} = 0.5AC_p(\lambda,\beta) \times \left(\frac{R\omega_{m_o pt}}{\lambda_{opt}}\right)^3 = K_{opt}(\omega_{m_o pt})^3 \tag{22}$$

Also the optimum torque calculated from the Eq. (23) is

$$T_{w_o pt} = K_{opt}(\omega_{m_o pt})^2 \tag{23}$$

Optimal Torque control adjusts the generator torque to its optimal at different wind speeds. However, it requires the knowledge of turbine characteristics (C_{pmax} and λ_{opt}). If the conditions are optimal, based on Eq. (23), the optimum speed of the rotor can be estimated as: Where K_{opt} is a constant determined by the wind turbine characteristics.

2.7. Three phase rectifier

The three phase rectifier unit consists of three legs and each leg consists of two diodes. The generated energy by the PMSG is supplied to the three phase rectifier to convert generated AC to DC. The average value of output voltage is (Rashid, 2007)

$$V_{OAV} = \frac{3}{\Pi}\int_{\Pi/3}^{2\Pi/3}\sqrt{2}V_L \sin\omega t(d\omega t) = \frac{3\sqrt{2}}{\Pi}V_L \tag{24}$$

2.8. Battery model

To study the performance of Battery connected hybrid system a generic model of rechargeable battery is used (Saw et al., 2014, https://in.mathworks.com). The model of Lead Acid battery the charging as well as discharging characteristic has to implement mathematically which follows the Eqs. (25) and (26).

$$V_{bat} = E_0 - Ri - k\frac{Q}{it - 0.1Q}.t^* - K\frac{Q}{Q - it}.it + \exp(t) \tag{25}$$

$$V_{batt} = E_0 - Ri - K\frac{Q}{Q - it}.(it + .t^*) + \exp(t) \tag{26}$$

where V_{bat} represents battery voltage (V), E_0 represents battery constant voltage (V), K represents polarisation constant (V/(Ah)) or polarisation resistance (Ω), Q represents battery capacity (Ah), it represents actual battery charge (Ah), A = exponential zone amplitude (V), B = exponential zone time constant inverse $(Ah)^{-1}$, R represents internal resistance (Ω), i represents battery current (A), i^* represents filtered current (*A*).

2.9. Operation of charge controller for the hybrid solar-wind off-grid power supply system

The design of a charge controller for a hybrid power sources based system is complicated compared to the single power source based off-grid distributed generation system.

To maintain the continuity of the energy flow and adequate protection to the equipments the modified version of charge controller has been depicted in Fig. 8 where SPV and WTG are acting as a sources of electrical energy. The primary requirement of synchronizing two different sources with a constant voltage source is to maintain the source voltages equal. As the sources are different in nature and the generated voltage by the different sources is not identical in nature a special charge controller is required to maintain desired energy flow. Due to different voltage the delivered energy circulating among the different sources and never synchronizes with the battery voltage. So the charging of the battery using different energy sources is hampering. In this case, two sets of battery bank solve the problem related to synchronization of two different energy sources to the battery. Here, the power output from the solar energy shares most of the power required by the load. The WTG based secondary source has delivered the energy to increase the reliability of the power supply system without increasing the size of the battery bank. In this proposed system the PV array acts as a primary source of energy. Based on the energy demand and the generated energy the battery is in charging or discharging mode. If the battery connected to the primary sources is unable to provide energy due to unavailability of the solar energy, the secondary sources provide the required energy to the consumer. As both of the energy sources is in synchronize with individual battery bank the entire generated energy is utilize which enhance the capacity of power supply system.

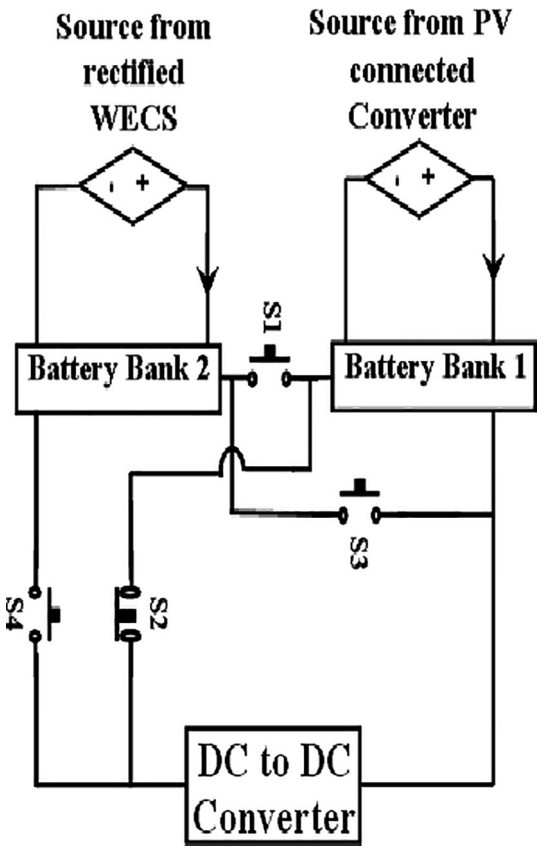

Fig. 8. Configuration of battery management for hybrid power supply system.

Fig. 9 indicates the related algorithm to maintain the battery charging, discharging, floating condition as well as protection of the appliance using four switching devices connected to the battery bank. At first the power level of the solar PV, the individual battery bank voltage and the SOC of the individual battery bank are measured and compared with a predefined value. At the initial, if the SOC of the battery and the generated power of the solar PV (SPV) is more than the reference value only switch S2 is ON and the battery bank 1 is connected to the load and the primary energy sources. Based on the energy supplied to the battery by the sources and the power supplied by the battery to the load the battery bank is in charging, discharging or in a floating condition. If the generated energy by the SPV is less than the predefined value the switch S3 and S4 are ON and the battery bank 2 is connected to the load. Here also the energy supplied by the secondary energy source (WTG) to the battery is maintained the charging, discharging or in floating condition based on the supplied energy from the source to the battery bank 2 and the energy consumed by the load. In the worst condition whenever both of the individual sources are unavailable to provide adequate energy to the battery bank the SOC of the battery individually checked and if the SOC is low compared to the predefined value the battery voltage has also been checked. As the battery bank voltage is directly linked with SOC for minimum SOC condition the voltage of the individual battery bank is very low both of the battery banks are connected in series

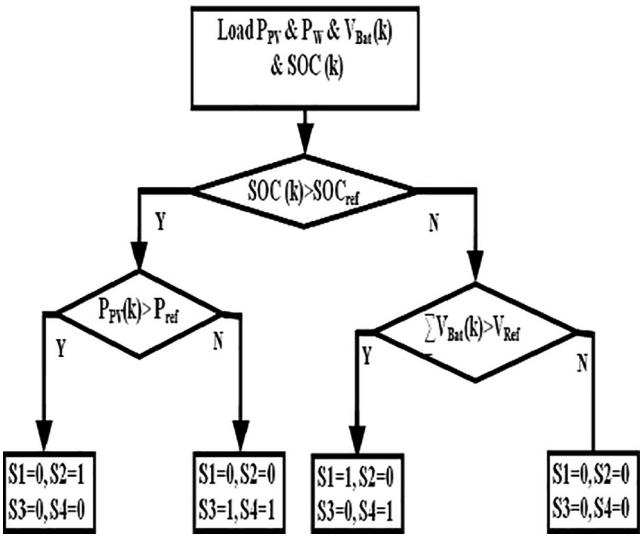

Fig. 9. Algorithm to maintain the optimum charging and discharging of the battery management system.

by switching on S1 and S4. If the SOC of the batteries is further reduced the battery bank is unable to maintain the required voltage and in that condition all the switches are in OFF condition and the load is thrown off. Here, during operation the charge controller maintains the hybrid system in a single source power supply system where either battery bank 1 or battery bank 2 is in operation. As the primary or the secondary sources of energy are always connected to the battery bank the generated energy is always transferred to the battery bank during standby condition also.

2.10. Boost converter

The boost converter has stepped up the battery voltage to a high level and supplied to the inverter. The stable high voltage obtained by the PI controlled boost converter increase the stability of the generated voltage of the inverter unit (Rashid, 2007; Zammit et al., 2017). The output voltage obtained by the boost converter is

$$V_{out} = V_{in}\left(\frac{1}{1-D}\right) \tag{27}$$

here, V_{in} is the input voltage of the Boost converter, V_{out} is the output voltage of the Boost converter, i_a is the average current at the load end, T is the cycle time period ($T = 1/f_s$), f_s is the switching frequency, L is the selected inductor value, D is the Duty cycle.

2.11. Three phase inverters

The inverter is a device which converts DC to AC with the desired frequency. A three phase bridge type Voltage source inverter (VSI) converts generated DC into three phase AC. The three legs of the inverter circuit consist of two MOSFET switch operated by specially designed PWM signals (Rashid, 2007; Michal, 2016). The Switches simultaneously ON and OFF using desired pulses obtained from pulse width modulation technique to generate balanced three phase output voltages to supply a three phase load. The PWM technique consists of three sinusoidal modulating signals with appropriate 120° phase shift, generated by the vector control circuit is compared with high frequency triangular carrier signal and generates the required pulses for switching operation. The line-to-line RMS voltage at the fundamental frequency, due

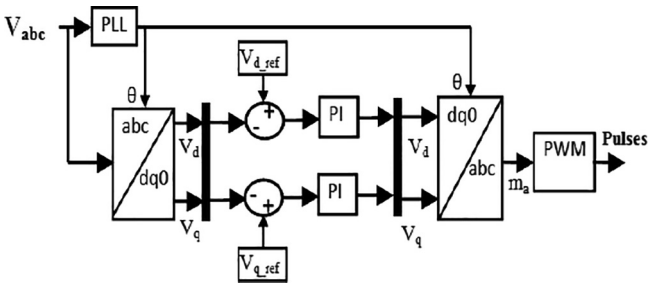

Fig. 10. Block diagram for PI voltage regulator.

to 120^0 phase the displacement between phase voltages can be written as

$$V_{ph} = \left(\frac{2\sqrt{2}}{\pi}\right).\cos\left(\frac{\pi}{6}\right).V_{dc} \tag{28}$$

where V_{ph} is the obtained phase voltage at the terminals, and V_{dc} is the input voltage of the inverter. The PID control PWM technique is utilised to generate desired pulses for the inverter.

2.12. Inverter controlled pulse generator circuit

To obtain the output voltage as desired value (three phase 400 Volt) a PI voltage regulator is introduced here, which maintains the desired voltage using space vector modulation controller. The vector control unit using a synchronous reference frame is based on the Clark and Park transformation to obtain the direct and indirect components of the voltage (Lee et al., 2014; Tran et al., 2016).

Fig. 10 indicates the pulse generator circuit for the inverter which maintains the desired voltage and frequency of the inverter under variable load condition. The model based on the synchronous reference frame and changes the firing angle of the different switches to obtain constant voltage and frequency at the inverter output.

The Phase lock loop (PLL) unit measures the reference angle of the synchronous reference frame. The voltage obtained at the inverter terminal is decomposed into the active component (V_d) and reactive components (V_q) using "abc to dq0" transformation. The difference between the decomposed quantity and the reference quantity is passes through the PI controller to modify the shape of the decomposed voltages profile. The V_d and V_q and V_0 (zero sequence component considered as zero) are further composed using to dq0 to abc transformation using the reference angle provided by the PLL which generates a duty cycle to generates a pulses using PWM technique.

3. Result and discussion

The standalone PV system generates electrical energy from the different irradiance of the Sun. To maximize the operating voltage 34 no's of solar panel is connected in series, which can deliver 14.79 kW power at maximum irradiance condition. To increase reliability of the supplied electricity, battery banks are attached to the system. To the capacity of the supplied electricity without increasing the size of the battery bank, WECS is also attached to the system as a secondary source of energy. The WECS generates electrical energy from the wind and the battery unit stores the generated electrical energy and supplied to the consumer when the primary energy sources are unable to deliver required electrical energy. A three phase rectifier is attached to the PMSM to rectify variable frequency electricity. The generated electricity from the

PV and the Wind then connected to a battery unit individually using a charge controller, which maintains the charging, discharging and floating condition and also provides protection of the battery bank. The charge controller also maintains the system as a single battery unit and connected to the PI controlled DC to DC converter. To increase the voltage of the battery a PI controlled boost converter is attached to the system. The voltage boost up is necessary to maintain the inverter input voltage constant which helps the inverter control system to maintain the load voltage as desired value. The inverter is connected to the boost DC-DC converter which converts DC to three phase AC with the desired quality using a simple LC filter. To study the overall system performance a variable solar irradiance (I_{rr}), wind speed (S_w) and variable load (P_{L1} = 16 kW, 0.95 pf, P_{L2} = 16 kW, 0.9 pf, P_{L3} = 16 kW, 0.85 pf) is applied in this present study and analyse the effectively of the proposed hybrid model which is indicated in Table 1.

The Table 1 indicates profile of the variable solar irradiance (I_{rr}), variable wind speed (S_w) and variable load with respect to time.

Fig. 11 indicates the performance of the PV array based on the variation of solar irradiance. Fig. 11(a) indicates the profile of the generated current, Fig. 11(b) indicates the profile of the generated voltage, Fig. 11(c) indicates the profile of the generated power by the PV array. At the initial condition the IC based MPPT controller performance is slow. The controller takes around 1.6 s to reach the maximum power around 10 kW due to 0.698 kW/m^2 solar irradiance. At 2.52 s the irradiance changes to the 0.928 kW/m^2 and the PV array generates 13.9 kW. After 4.52 s the irradiance changes to 0.378 kW/m^2 and the PV array generates 5.8 kW electricity.

In this proposed system a PMSG is attached to the wind turbine to generate electrical energy from the wind. Fig. 12 indicates the performance of the PMSG under variable wind speed. Fig. 12(a) indicates the instantaneous voltage profile of the PMSG and Fig. 12(b) indicates the instantaneous current profile of the generated current generated by the PMSG. The voltage quantity of the PMSG almost constant only the current quantity changes with the change in wind speed.

Table 1
Variation of solar irradiance and wind speed used in this study.

Time (s)	0–2.52	2.52–4.52	4.52–6.00
I_{rr} (kW/m^2)	0.698	0.928	0.378
Time (s)	0–1.69	1.69–4.00	4.00–6.00
S_w (m/s)	10.32	8.00	11.49
Time	0–3	3–5	5–6
Connected Load (kW)	P_{L1}	P_{L1}, P_{L2}, P_{L3}	P_{L1}, P_{L2}

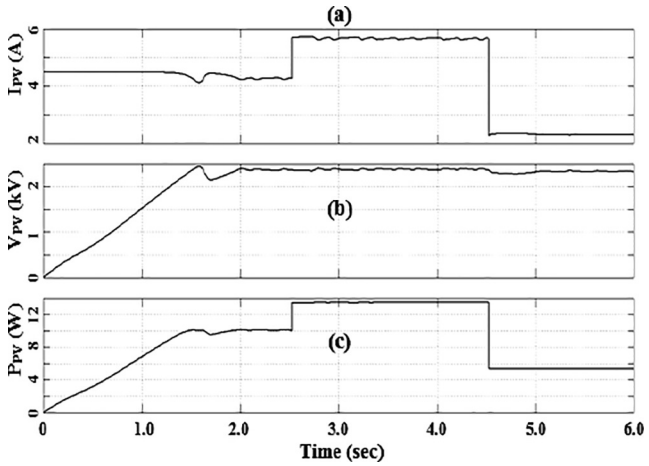

Fig. 11. Generated (a) voltage (b) current (c) power profile of the PV array under variable irradiance of the Sun.

Fig. 13 indicates the performance of the rectifier connected to the PMSG. The generated electrical energy by the PMSG is variable frequency in nature. Hence a rectifier unit is necessary to supply the generated energy to the battery. Fig. 13(a) indicates the profile

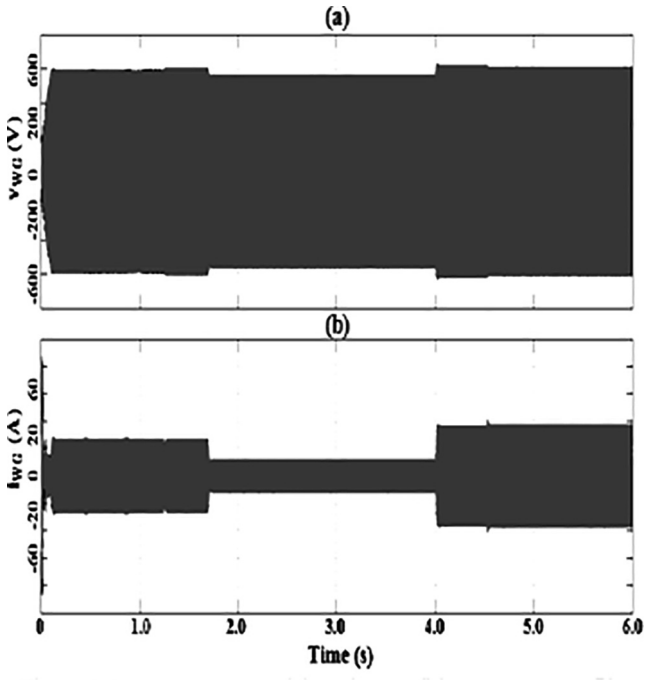

Fig. 12. Instantaneous (a) voltage (b) current profile of the PMSG connected with WT.

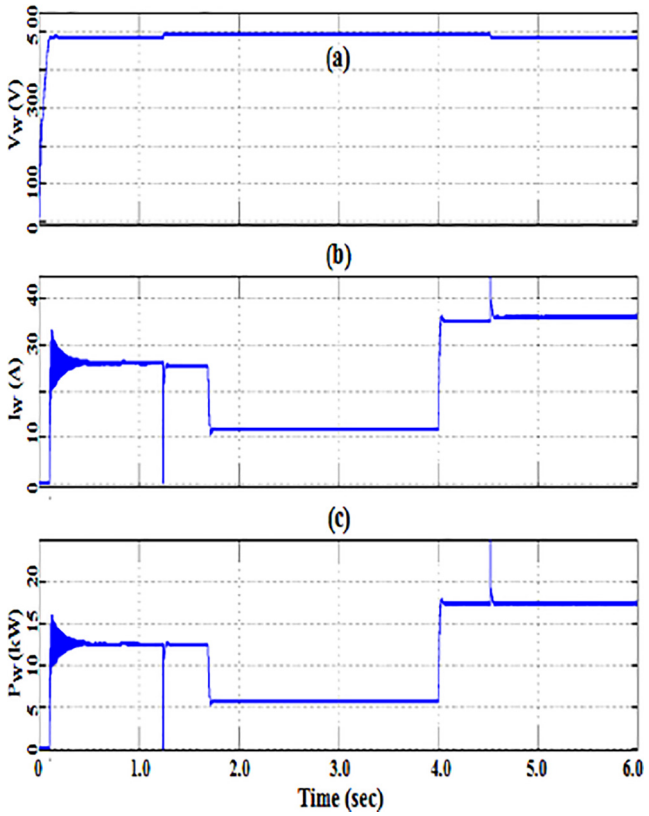

Fig. 13. The rectified (a) voltage (b) current (c) power profile of the PMSG connected with WT.

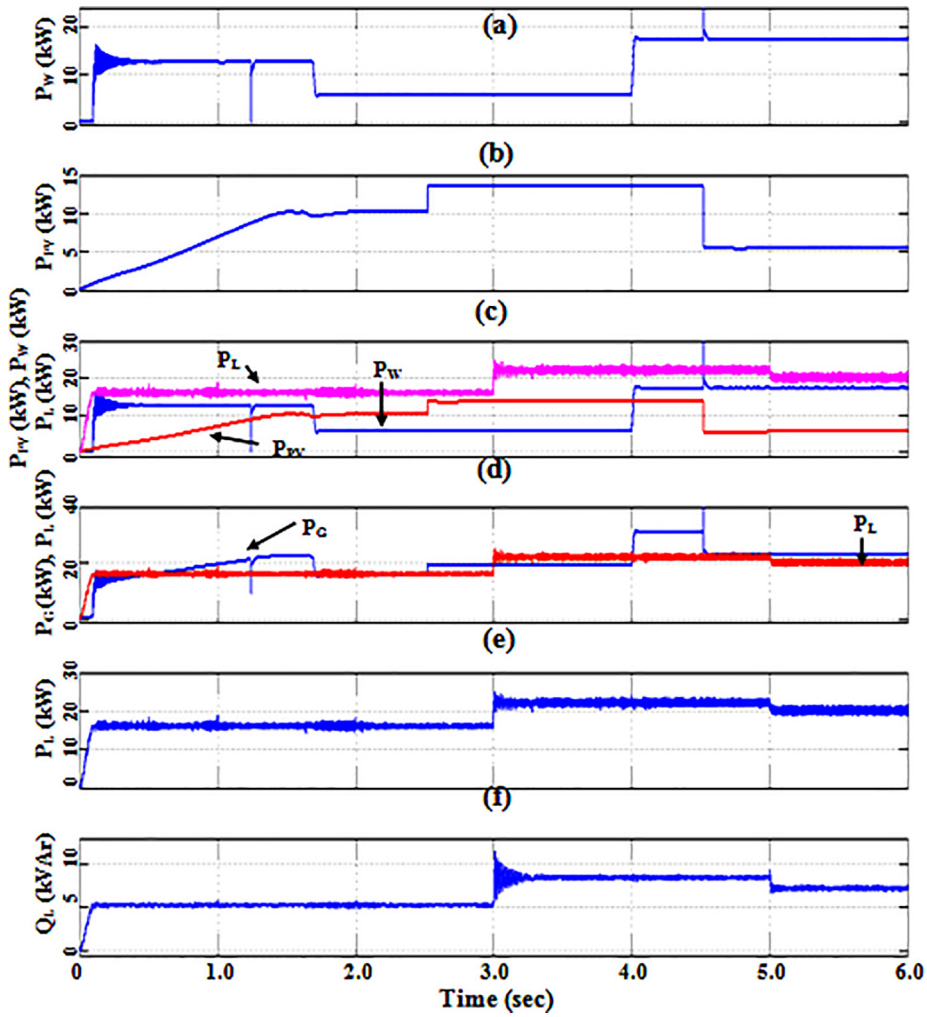

Fig. 14. Generated and connected load profile (a) power generated by WTG (P_w) (b) power generated by PV array (P_{PV}) (c) comparison of generated power and consumed power (d) comparison of total generated power (P_G) and consumed power (P_L) (e) active power profile of the load (f) reactive power profile of the load.

of the rectified voltage, Fig. 13(b) indicates the profile of the rectified current, Fig. 13(c) is indicates the profile of the rectified power output due to variable wind speed. Except the initial time the OTC based MPPT controller performance will satisfactory. At the initial condition the PMSG generates power around 13.5 kW due to 10.32 m/s wind speed. At 1.69 s the wind speed reduced to 8 m/s and the PMSG generates 5.3 kW. After 4 s the wind speed changes to 11.49 m/s and the PMSG generates 17 kW.

Fig. 14(a) indicates the generated power from the PV array under variable solar irradiance, Fig. 14(b) indicates the generated power by the WTG set under variable wind speed, Fig. 14(c) indicates the comparison of generating power as well as consumed power, Fig. 14(d) indicates the comparison of total generated power by the PV and WTG and the power consumed by the load. Fig. 14(e) and (f) indicates the active and reactive power profile of the load. From Fig. 14(c) it is evident that the generated power by the PV array (P_{PV}) and the generated power by the PMSG (P_W) are low compared to the consumed load power (P_L). Fig. 14(d) indicates that the total generated power (P_G) is comparable with the Load power (P_L). Whenever the generated power P_G is low compared to the load power P_L the battery is in discharging mode, and whenever the generated power P_G is more compared to the load power P_L the battery is in charging mode. If the generated power (P_G) and the consumed power (P_L) are equal, the battery is in floating condition.

Fig. 15 indicates the load voltage profile under variable load condition. Fig. 15(a) indicates the instantaneous three phase voltage profile which is constant for steady as well as load variation except for the small initial and switching condition of the connected load. Fig. 15(b) clearly indicates the increments and decrement of the load as the instantaneous three phase load current profile changes dependent upon the load demand. Fig. 15(c) indicates the RMS voltage per phase, which is constant for all the simulation time and Fig. 15(d), indicates the line current per phase. Depending upon the load variation the current quantity changes, but the phase voltage is constant for the entire simulation time.

To clarify the instantaneous voltage and current profile during the change in load Fig. 15 is enlarged during the change in load and indicated in Fig. 16. Here Fig. 16(a) indicates the instantaneous three phase voltage profile; Fig. 16(b) indicates the instantaneous three phase load current profile. At the initial time the voltage gradually increases and stabilizes at 230 V per phase within 0.095 sec. The current quantity also changes within 0.095 s and stabilized at around 24.3 A per phase. From the Fig. 6.15 it is observed that the time of insertion of the load L_2 and L_3 the load voltage is constant during the change in load, but the per phase

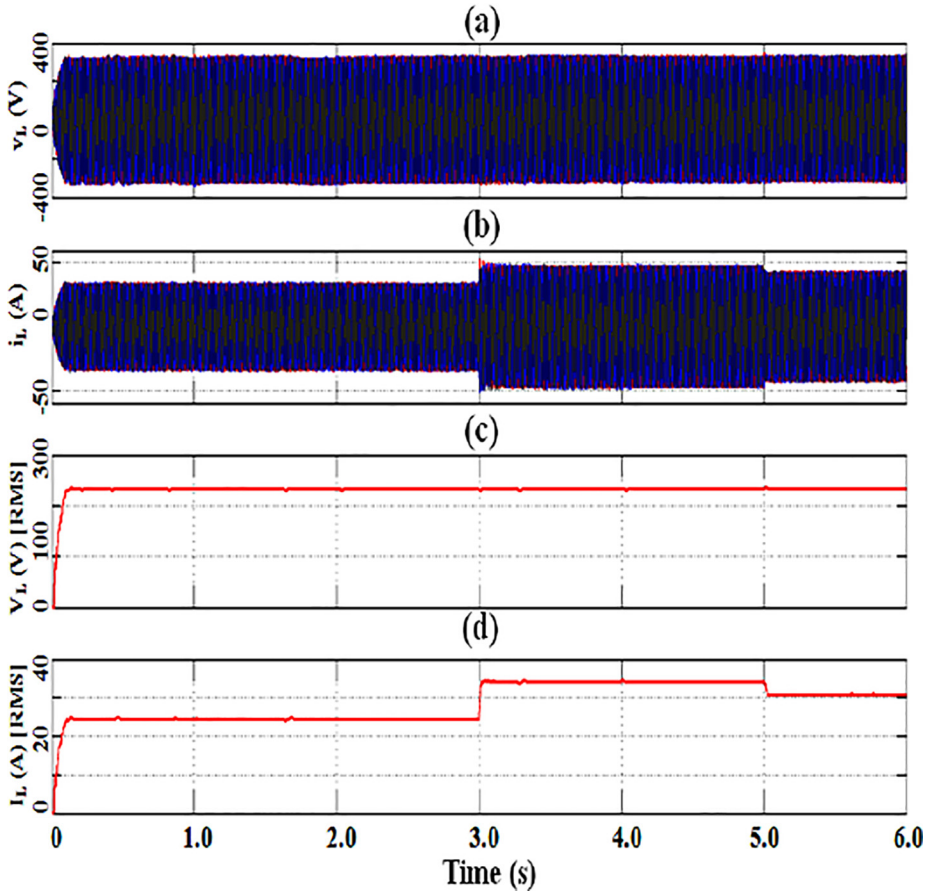

Fig. 15. Dynamic response of dc-ac converter with variable load (a) instantaneous voltage (b) instantaneous current (c) RMS voltage (d) RMS current profile.

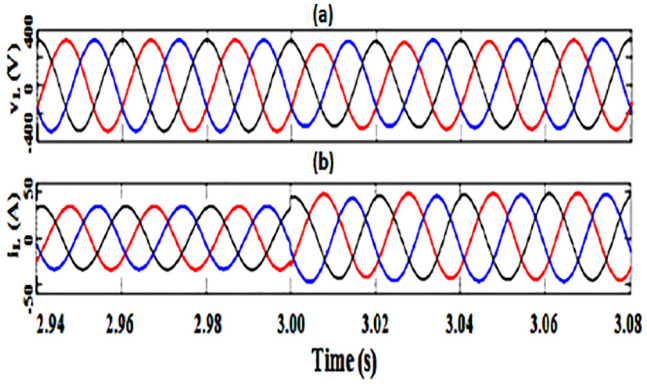

Fig. 16. Dynamic response of dc-ac converter with load increase (a) instantaneous voltage, (b) instantaneous current.

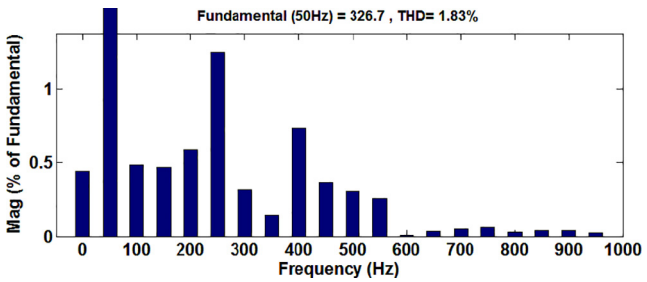

Fig. 17. Harmonic spectrum of load voltage.

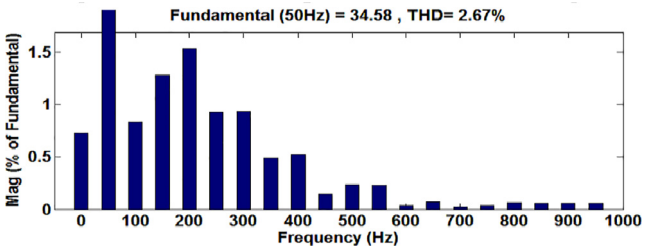

Fig. 18. Harmonic spectrum of load current.

current changes within 0.015 s and stabilizes to around 34 A during maximum load condition. After analysing the Fig. 6.16 it is clearly stated that during the exclusion of L_3 load the voltage is stable and the current profile stabilizes within 0.025 s and drawing 30.08 A constant current.

Figs. 17 and 18 indicate the harmonic spectrum of load voltage and current. In the proposed system the total harmonic distortion (THD) is around 1.93% for the voltage profile and 1.83% for the current profile which is very much lower as per IEEE 512-1992 standard. In the proposed system, as the quality power is obtained by using simple LC filter which minimize the overall system cost and increase the acceptability of the proposed system.

4. Conclusions

In this present study a standalone hybrid power system using solar and wind energy is successfully constructed. Both the MPPT

controller performance is satisfactory under variable irradiance and wind speed and maintains maximum power from the energy sources. The converter and the inverter unit has successfully maintains the power quality as per the standard. The charge controller for the hybrid power management performance is satisfactory. The hybrid battery management system maintains the energy flow to the load using different switches connected with the system. The different battery system maximizes the energy intake from the renewable energy sources and maintains reliable power to the consumer with the minimum battery capacity.

Appendix

Tables 2 and 3

Table 2
Parameters of wind energy conversion system (WECS).

Emulated wind turbine	
Number of blades	3
Air density (kg/m^2)	1.225
Diameter (m)	7.13
PMSG	
Stator resistance-*Rs* (Ω)	0.085
Armature inductance (H)	0.00095
Flux linkage-φv (Wb)	0.192
Torque constant	1.152
Voltage constant	139.2998
Number of pole pairs-p	6
Moment of inertia-*Jg*(kg·m^2)	0.008
Coefficient of friction-*Kg* (Nm·s/rad)	0.001147

Table 3
Specifications of SPR-E20-435-COM module under STC.

Parameter of the solar panel	
Maximum Power (W)	435
Open Circuit Voltage (V)	85.6
Maximum Power Point Voltage (V)	72.9
Short Circuit Current (A)	6.43
Maximum Power Point Current (A)	5.97

References

Arifujjaman, M., 2010. Modeling, simulation and control of grid connected Permanent Magnet Generator (PMG)-based small wind energy conversion system. IEEE Electr. Power Energy Conf. 2010, 1–6.

Commercial Solar Panels E20-435-COM. https://us.sunpower.com/sites/.../data.../ds-e20-series-435-commercial-solar-panels.pdf. (Accessed 13 November 2017).

Ebrahimi, M.J., 2015. General overview of maximum power point tracking methods for photovoltaic power generation systems. Int. Power Syst. Conf., 136–141

Generic model of a battery. https://in.mathworks.com/help/physmod/sps/powersys/ref/battery.html?s_tid=gn_loc_drop. (Accessed 03 October 2017).

Hur, S., 2018. Modelling and control of a wind turbine and farm. Energy 156, 360–370.

Jamal, T., Urmee, T., Calais, M., Shafiullah, G.M., Carter, C., 2017. Technical challenges of PV deployment into remote Australian electricity networks: a review. Renew. Sustain. Energy Rev. 77, 1309–1325.

Jena, D., Rajendran, S., 2015. A review of estimation of effective wind speed based control of wind turbines. Renew. Sustain. Energy Rev. 43, 1046–1062.

Kamran, M., Mudassar, M., Fazal, M.R., Asghar, M.U., Bilal, M., Asghar, R., mran et al. 2018. Implementation of improved Perturb & Observe MPPT technique with confined search space for standalone photovoltaic system. J. King Saud Univ. – Eng. Sci.

Lee, K.J., Lee, J., Shin, D., Yoo, D., Kim, H., 2014. A novel grid synchronization PLL method based on adaptive low-pass notch filter for grid-connected PCS. IEEE Trans. Industr. Electr. 61 (1), 292–301.

Michal, V., 2016. Three-Level PWM floating H-Bridge Sine wave power inverter for high-voltage and high-efficiency applications. IEEE Trans. Power Electr. 31 (6), 4065–4074.

Panwar, N.L., Kaushik, S.C., Kothari, S., 2011. Role of renewable energy sources in environmental protection: a review. Renew. Sustain. Energy Rev. 15 (3), 1513–1524.

Rashid, M.H., 2007. Power Electronics Handbook. Elsevier, USA.

Saw, L.H., Somasundaram, K.K., Ye, Y., Tay, A.A.O., 2014. Electro-thermal analysis of Lithium Iron Phosphate battery for electric vehicles. J. Power Sources 249, 231–238.

Taleb, M., 2004. Optimal operation of a wind driven system. J. King Saud Univ. – Eng. Sci. 16 (2), 229–251.

Tran, Q., Truong, A.V., Le, P.M., 2016. Reduction of harmonics in grid-connected inverters using variable switching frequency. Int. J. Electr. Power Energy Syst. 82, 242–251.

Wu, Z., Dou, X., Chu, J., Hu, M., 2013. Operation and control of a direct-driven PMSG-based wind turbine system with an auxiliary parallel grid-side converter. Energies 6, 3405–3421.

Xiaodong, W., Shixu, H., Shirong, W., Yingming, L., Lixia, L., 2013. Multi-objective optimization torque control of wind turbine based on LQG optimal control. 25th Chinese Control Decision Conf. (CCDC), 405–408.

Zammit, D., Staines, C.S., Micallef, A., Maurice, A., Lieari, J., 2017. Incremental current based MPPT for a PMSG micro wind turbine in a grid-connected DC microgrid. Energy Procedia. 142, 2284–2294.

Zhihui, Ren, Zhongdong, Yin, Bao, W., 2009. Control Strategy and Simulation of Permanent Magnet Synchronous wind Power Generator. Environment Technology, pp. 568–571.

Zoua, C., Zhao, Q., Zhang, G., Xiong, B., 2016. Energy revolution: from a fossil energy era to a new energy era. Natl. Gas Industry B. 3 (1), 1–11.